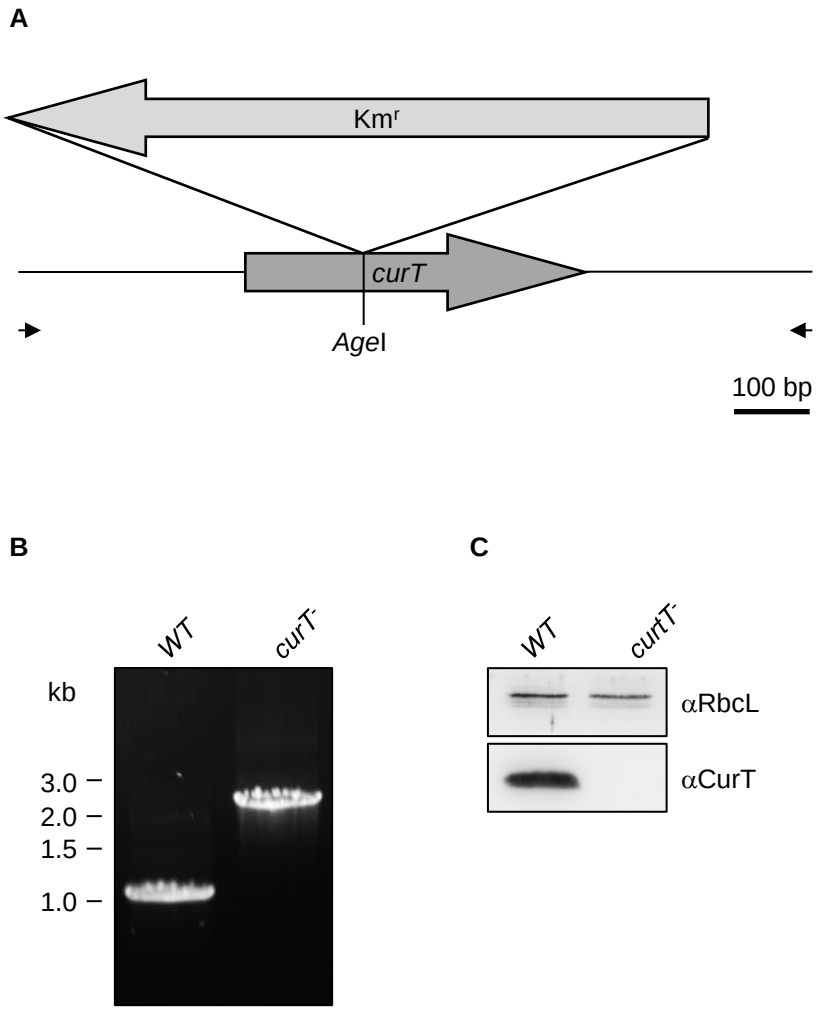

Supplemental Figure 1. Construction of the *curT*$^-$ mutant. **A)** Strategy for inactivation of *curT*. The donor plasmid used to generate CurT-deficient lines is shown schematically, with the kanamycin resistance cassette inserted at the unique *Age*I site in the *curT* coding region. The open arrows indicate transcriptional orientation. Solid arrows mark the positions of primers which were used for the PCR-based segregation analysis of wild-type and *curT*$^-$ DNA depicted in **B**. **C)** Complete absence of the CurT protein in the mutant was verified by immunoblotting. As a loading control, the RbcL subunit of the Rubisco enzyme was analyzed in parallel.

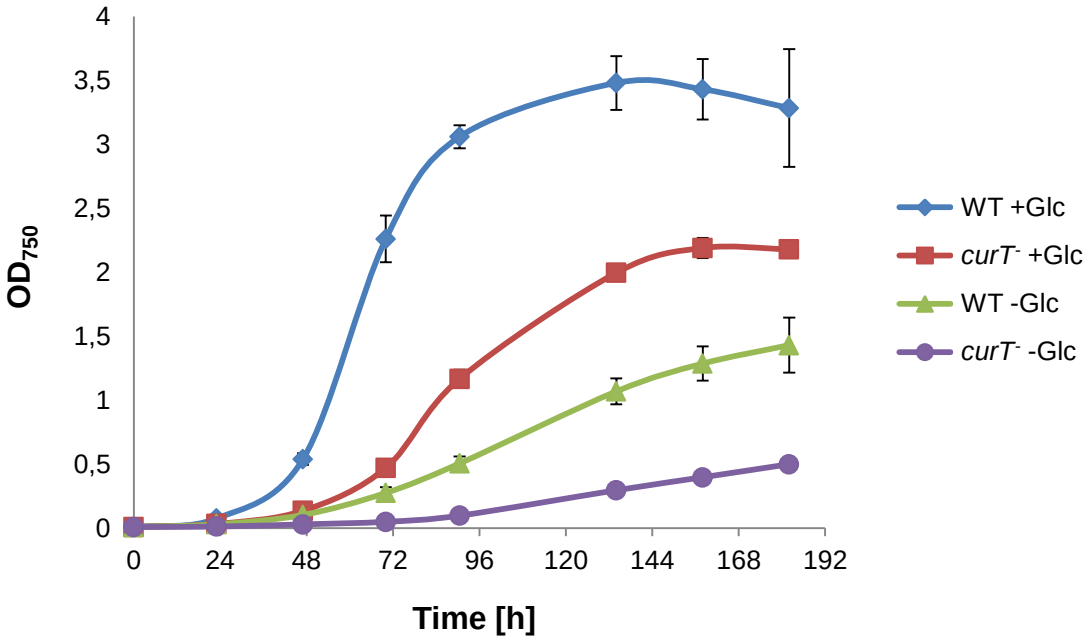

Supplemental Figure 2. Growth phenotype of *curT*$^{-}$. Wild-type and *curT*$^{-}$ cultures were grown in the presence and absence of glucose at 30 °C. Cultures were inoculated to OD_{750}=0.01 and the OD_{750} was monitored every day. Data are means ± SD of three independent experiments.

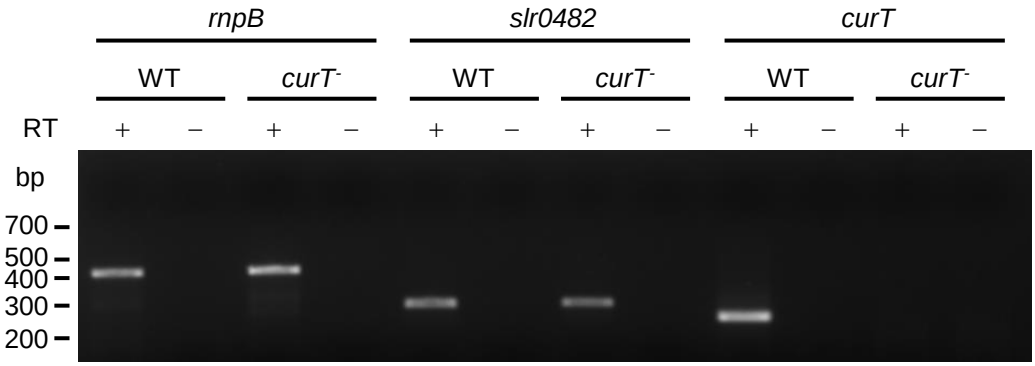

Supplemental Figure 3. Expression analysis of the open reading frame *slr0482* (located upstream of *curT*) in the *curT*- strain. RT-PCR analysis of mRNAs from wild-type or *curT*- cells, performed using primer pairs specific for *rnpB*, *slr0482* or *slr0483* (*curT*). Note that expression of *slr0482* is unaffected by the status of the *curT* locus, and that the *curT*- mutant does not express *curT* RNA. A negative control without reverse transcriptase (RT) was performed for each reaction. The expression of *rnpB*, which is the catalytic RNA component of the tRNA-processing Rnase P, served as control (Vioque, 1992).

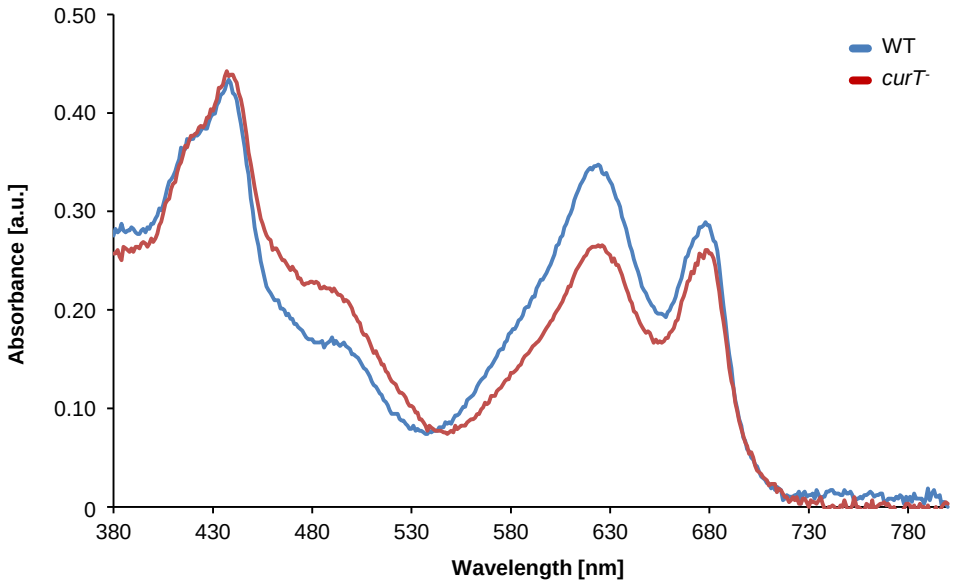

Supplemental Figure 4. Absorbance spectra of *curT*$^{-}$ and wild-type cells. Spectra were normalized to the OD_{750}. Cells were grown at 30 µmol photons $m^{-2}s^{-1}$ in BG11 with 5 mM glucose.

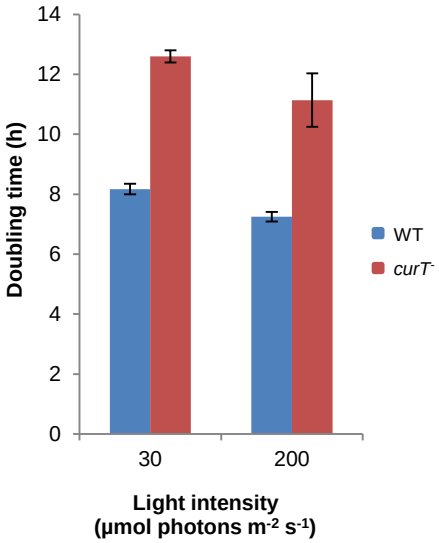

Supplemental Figure 5. High-light growth phenotypes of wild-type *Synechocystis* 6803 and the *curT*$^-$ strain. Cultures of wild-type and *curT*$^-$ cells were inoculated to OD_{750}=0.01 and grown in the presence of glucose at 30 °C and 200 µmol photons $m^{-2}s^{-1}$. Doubling times were calculated based on the OD_{750} after two days. Doubling times are mean ± SD of three independent experiments.

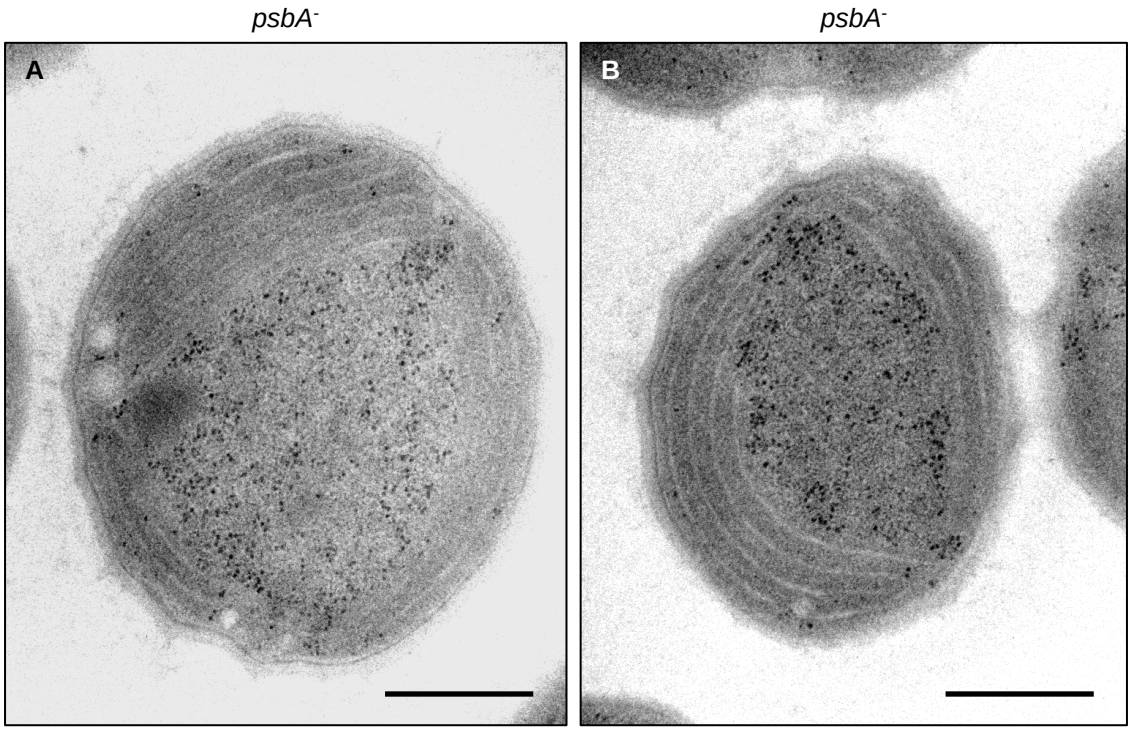

Supplemental Figure 6. Ultrastructure of the *TD41* mutant, which lacks the *psbA* transcript and the D1 protein. Scale bar: 500 nm.

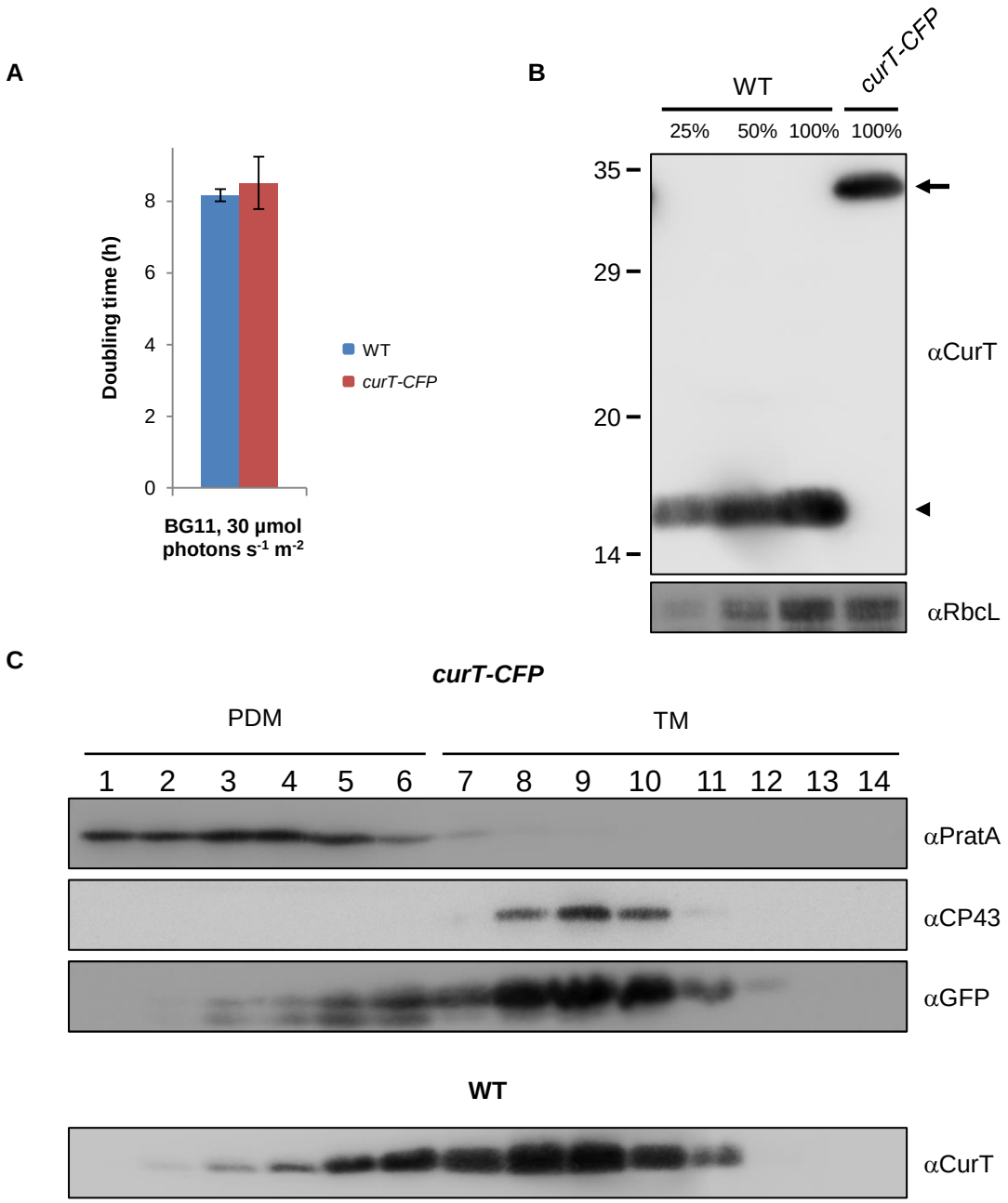

Supplemental Figure 7. Expression and localization of CurT-CFP. **A)** Growth of wild-type *Synechocystis* 6803 and the *curT-CFP* strain under normal lighting conditions. **B)** Comparison of the expression level of CurT-CFP with that of CurT in the wild type demonstrates the complete absence of untagged CurT in *curT-CFP* cells. The arrow and arrowhead indicate the position of CFP-tagged CurT and native CurT, respectively. To control for equal loading, the blot was probed with an αRbcL antibody. Quantification of three independent experiments confirmed wild-type like expression levels of CurT-CFP (96±16 %). **C)** Membrane fractionation confirms that CurT-CFP behaves just like wild-type CurT. Controls and detection of the CurT-CFP fusion protein by αGFP indicates a protein distribution which is not affected by the CPF-tag. For ease of comparison, the distribution of wild-type CurT from Figure 7 is included below that of the fusion protein.

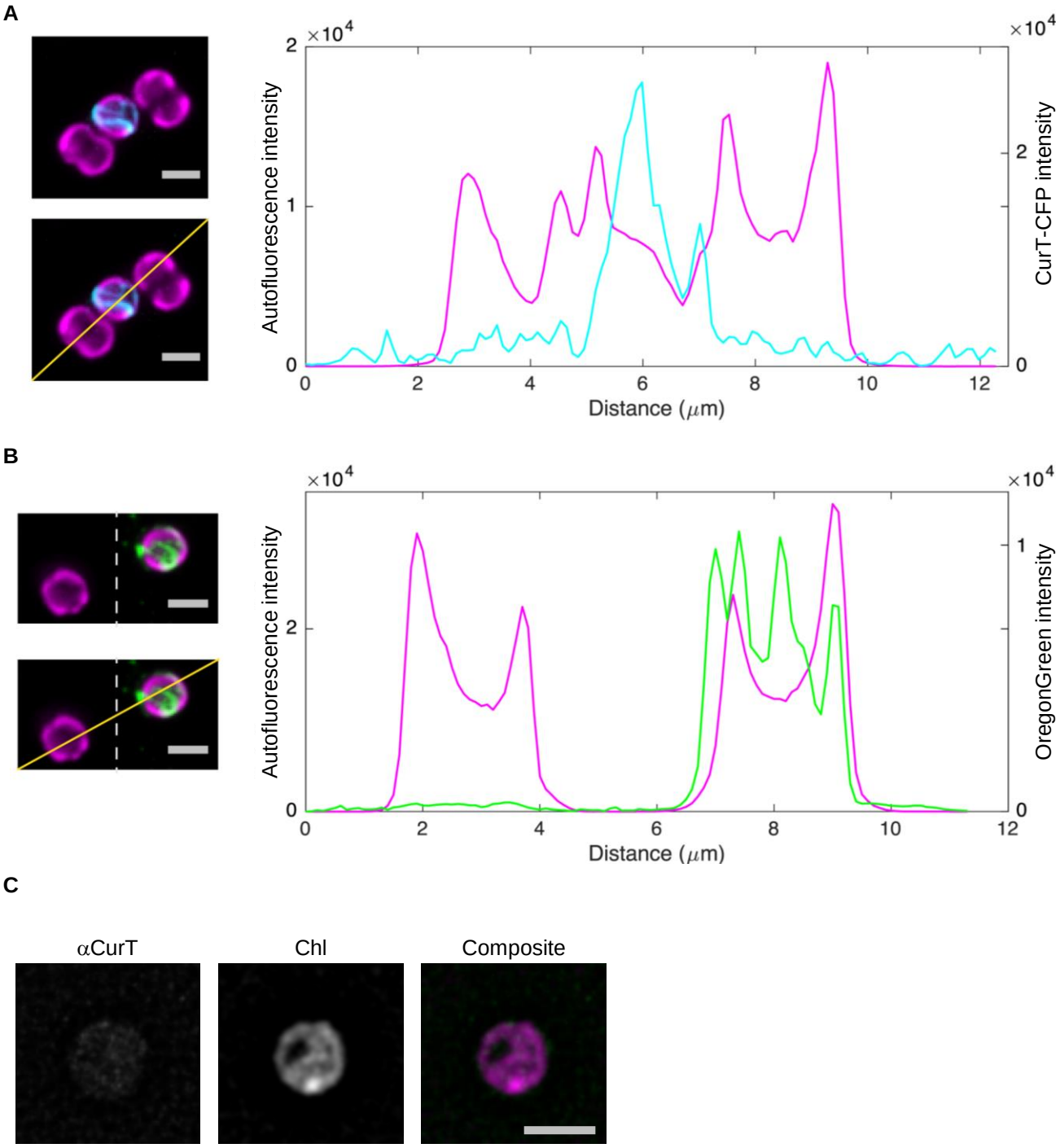

Supplemental Figure 8. Localization of CurT and CurT-CFP by fluorescence microscopy. **A)** Wild-type and *curT-CFP* cells were mixed to show the relative intensity of the CurT-CFP signal. Images are maximum projections and were quantified on a diagonal line profile. **B)** Cells treated or not treated with αCurT as primary antibody were combined in one image. As in **A)** a diagonal line profile traversing both cells shows the intensity of the signal in the imaging channel. **C)** Negative control. Immunofluorescence of *curT*$^{-}$ mutant probed with αCurT antibody. Scale bars: 2 µm.

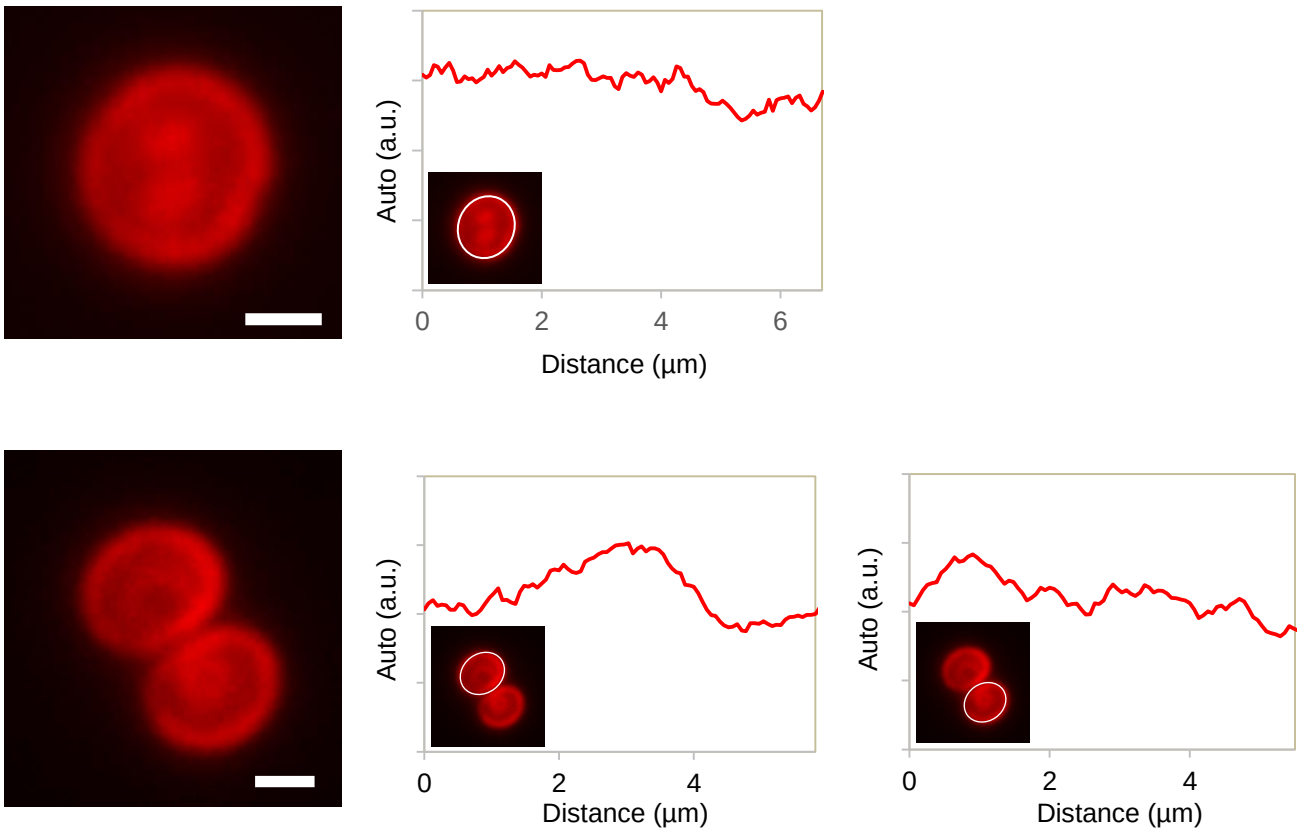

Supplemental Figure 9. Chlorophyll autofluorescence of *curT*$^-$. For exemplified live-cell imaging of the *curT*$^-$ mutant, cells were processed exactly as in Figure 8. The chlorophyll autofluorescence is shown in red. Fluorescence intensity profiles of the cell's periphery are depicted on the right. Scale bars: 1 µm.

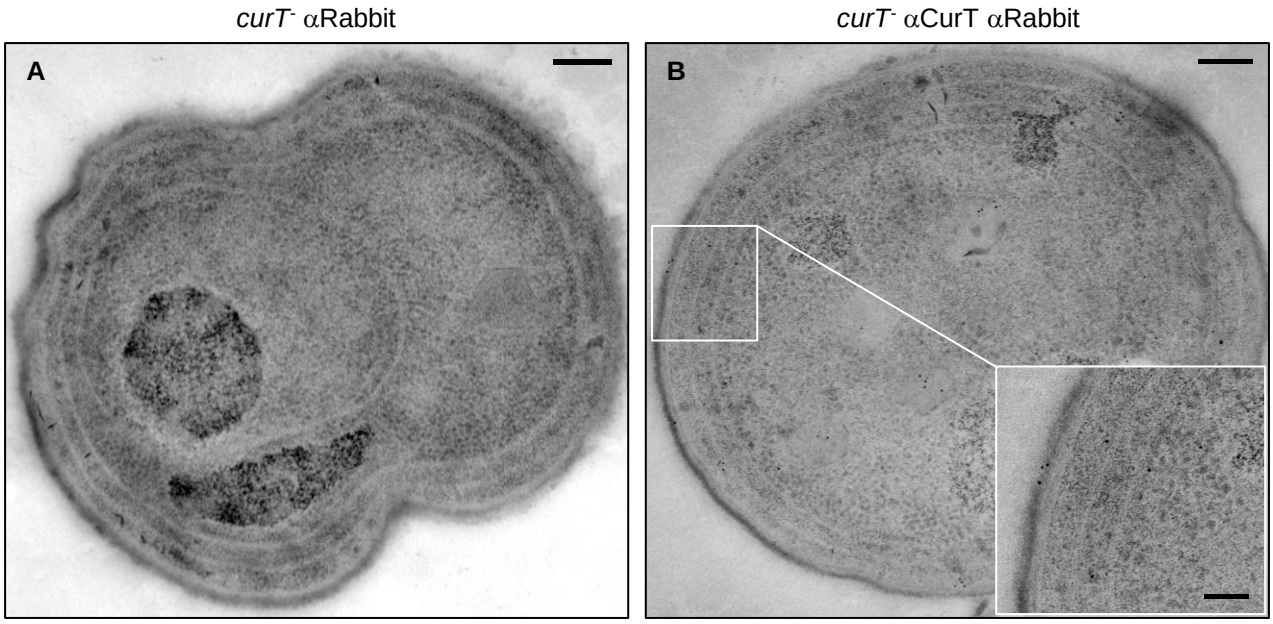

Supplemental Figure 10. The *curT*- mutant as a negative control for immunogold labeling. Ultrathin sections of *curT*- cells that had **(B)** or had not **(A)** been exposed to the primary antibody rabbit αCurT (1:500) and were then treated with gold-conjugated goat anti-rabbit IgG served as an additional negative control for the subcellular localization of CurT by immunogold labeling. Bars = 200 nm (overview) and 100 nm (details), respectively.

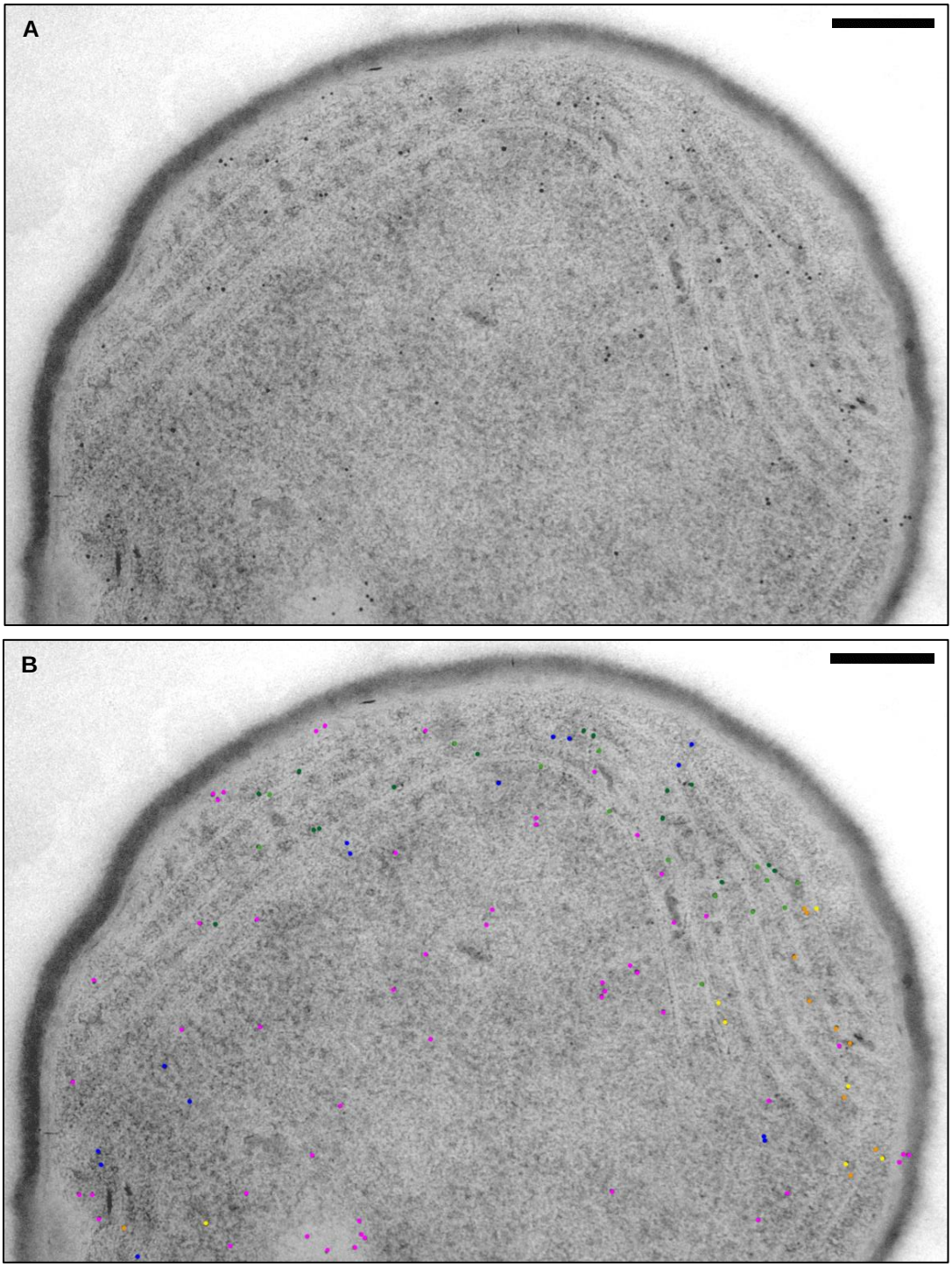

Supplemental Figure 11. Representative counts of immunogold signals. **A)** Detailed view of a wild-type ultrathin section labeled with αCurT (cell from Figure 10B, rotated 90°) and color-coded analysis of the same cell (**B**). The colors highlight the localization of each signal: dark green: convex side of green region; light green: concave side of green region; dark yellow: convex side of yellow region; light yellow: concave side of yellow region; blue: no reliable assignment possible; magenta: not located at thylakoid membrane. Scale bars represent 200 nm.

Supplemental Table 1. Overview of immunogold signals in *curT*$^{-}$ cells.

	Total number of signals		Relative number of signals	
	convex	concave	convex	concave
Total thylakoid membrane	185	179	50.8	49.2

The analysis of the *curT*$^{-}$ mutant was performed identically to the wild-type (Supplemental Figure 9) and revealed a total number of 364 signals which are located at the thylakoid membrane in 30 cells. Discrimination between different regions of the thylakoid membrane was not possible in the *curT*$^{-}$ mutant, due to the absence of biogenesis centers. Statistical analysis by the χ^2 test as performed for the wild-type signals (Supplemental Table 3) confirmed a random distribution to the convex and concave side of the thylakoid membrane.

Supplemental Table 2. Overview of immunogold signals in specific regions of *Synechocystis* 6803 wild-type cells.

	Total number of signals		Relative number of signals	
	convex	concave	convex	concave
Total thylakoid membrane	888	696	56.1	43.9
Green regions	499	413	54.7	45.3
Red regions	201	163	55.2	44.8
Yellow regions	188	120	61.0	39.0

Quantification of immunogold signals after labeling with αCurT as primary antibody in 95 cells resulted in the total of 1584 signals, which are unambiguously located at the thylakoid membrane and can be assigned to either the convex or the concave side of the thylakoid lamella. The relative numbers of immunogold signals were calculated for total thylakoid membranes and each specific membrane region as shown in Figure 10F and Figure 10G.

Supplemental Table 3. Statistical analysis of immunogold signals for wild-type *Synechocystis* 6803 cells.

	Total TM	Green	Red	Yellow
Deviation from random distribution	***	**	*	***
Deviation from total TM distribution	X	-	-	***
Deviation from green distribution	-	X	-	***
Deviation from red distribution	-	-	X	*
Deviation from yellow distribution	***	***	*	X

The null hypothesis of a random 50:50 distribution was tested for the observed distributions of immunogold signals on the convex and concave sides of the thylakoid membrane in the defined regions (Supplemental Table 2). Each hypothesis was compared pairwise to the entire thylakoid membrane, as well as the different regions, by performing a χ^2 test (Zöfel, 1988). The asterisks indicate significant differences to the corresponding hypothesis (df = 1) with error probabilities of <5 % (*), <1 % (**) and 0.1 % (***); - no significant difference.

Supplemental Table 4. Co-expression of *curT*.

ORF	Function
slr1945	2,3-bisphosphoglycerate-independent phosphoglycerate mutase, yibO, pgm, slr1945
ssr3451	cytochrome b559 alpha subunit, psbE, ssr3451
sll0427	photosystem II manganese-stabilizing polypeptide, psbO
slr2094	fructose-1,6-/sedoheptulose-1,7-bisphosphatase, fbpI, glpX
smr0006	cytochrome b559 b subunit, psbF, smr0006
slr2073	hypothetical protein YCF50, ycf50, cdv2, sepF
smr0007	photosystem II PsbL protein, psbL, smr0007
sll0047	hypothetical protein YCF12, ycf12, psb30
slr1329	ATP synthase beta subunit, atpD, atpB
slr2067	allophycocyanin alpha subunit

Co-expression of CurT was examined using the CyanoEXpress 2.2 database (Hernández-Prieto and Futschik, 2012; Hernández-Prieto et al., 2016). The first ten hits in CyanoEXpress 2.2 are listed, which represent the genes whose expression profiles are most similar to that of *curT*.

Supplemental Methods

RT-PCR

RNA from *Synechocystis* 6803 wild-type and *curT*$^-$ cells was isolated using the TRI Reagent (Sigma-Aldrich, Munich, Germany) according to the manufacturer's instructions, and subsequently treated with RQ1 RNase-free DNase (Promega, Mannheim, Germany). Reverse transcription was performed with SuperScript III Polymerase (Invitrogen, Life Technologies GmbH, Darmstadt, Germany) followed by PCR-based cDNA amplification using gene-specific primers for *curT* (RT0483/5: AAG GAT CCG TGG GCC GTA AAC ATT CA; RT0483/3: AAG TCG ACA ATG AGG GGT TGC TTG TT), *slr0482* (RT0482/5: TGG GGG ATG CCT AGT TAT; RT0482/3: CCA GGG CTT TTC CAC TTT) and *rnpB* (RTrnpB/5: GAG AGT TAG GGA GGG AGT; RTrnpB/3: GAG AGT TAG TCG TAA GCC G).

Whole cell absorbance spectra

Whole cell absorbance spectra were measured with a Shimadzu UV-2450 UV-VIS spectrophotometer equipped with an ISR-2200 integrating sphere attachment which allows transmittance measurements of turbid samples with less than 0,015 % stray light. Prior to the measurement, cells were washed with BG11 medium and concentrated to an optical density at 750 nm (OD_{750}) of about 2 that was determined using a Beckman DU 7400 spectrophotometer. Spectra were normalized to an OD_{750} value of 1.

Supplemental References

Hernandez-Prieto, M. and Futschik, M.E. (2012) CyanoEXpress: a web database for interactive exploration and visualisation of the integrated transcriptome of cyanobacterium *Synechocystis* sp. PCC6803. Bioinformation **8**, 634-638.

Hernández-Prieto, M.A., Semeniuk, T.A., Giner-Lamia, J., and Futschik, M.E. (2016). The Transcriptional Landscape of the Photosynthetic Model Cyanobacterium *Synechocystis* sp. PCC6803. Scientific Reports **6,** 22168.

Tamura, K., Peterson, D., Peterson, N., Stecher, G., Nei, M., and Kumar, S. (2011). MEGA5: Molecular evolutionary genetics analysis using maximum likelihood, evolutionary distance, and maximum parsimony methods. Mol Biol Evol **28,** 2731-2739.

Vioque, A. (1992). Analysis of the gene encoding the RNA subunit of ribonuclease P from cyanobacteria. Nucleic Acids Res **20**, 6331-6337.

Zöfel, P. (1988). Statistik in der Praxis. (Stuttgart, Germany: Gustav Fischer Verlag).